ACS APPLIED MATERIALS & INTERFACES

Research Article

www.acsami.org

Direct Epitaxial Integration of the Ferromagnetic Semiconductor EuO with Silicon for Spintronic Applications

Dmitry V. Averyanov, Yuri G. Sadofyev, Andrey M. Tokmachev, Alexey E. Primenko, Igor A. Likhachev, and Vyacheslav G. Storchak*

National Research Center "Kurchatov Institute", Kurchatov Square 1, Moscow 123182, Russia

Supporting Information

ABSTRACT: Following a remarkable success of metallic spintronics, tremendous efforts have been invested into the less developed semiconductor spintronics, in particular, with the aim to produce three-terminal spintronic devices, e.g., spin transistors. One of the most important prerequisites for such a technology is an effective injection of spin-polarized carriers into a nonmagnetic semiconductor, preferably one of those currently used for industrial applications such as Si—a workhorse of modern electronics. Ferromagnetic semiconductor EuO is long believed to be the best candidate for integration with Si. Although EuO proved to offer optimal conditions for effective spin injection into silicon and in spite of considerable efforts, the direct epitaxial stabilization of stoichiometric EuO thin films on Si without any buffer layer has not been demonstrated to date. Here we report a new technique for control of EuO/Si interface on submonolayer level. Using this technique we solve a long-standing problem of direct epitaxial growth on silicon of thin EuO films which exhibit structural and magnetic properties of EuO bulk material. This result opens up new possibilities in developing all-semiconductor spintronic devices.

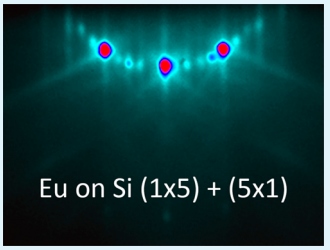

KEYWORDS: *magnetic semiconductors, europium monoxide, silicon, heteroepitaxy, spintronics*

INTRODUCTION

Strong correlation of spin and charge degrees of freedom in the same material makes it possible to manipulate magnetically stored information with electric fields and/or modify fast logic gates by changing the magnetization of their components. In metal multilayers such effects are manifest in giant magnetoresistance.[1,2] Metallic spintronic devices, such as hard disk read heads and magnetic random access memory, are among the most successful technologies of the past decades. However, metals cannot enhance signals—the prerequisite for transistor technology readily offered by semiconductors.

The development of semiconductor spintronics requires the ability to inject, modulate, and detect spin-polarized carriers in a single device, preferably made of technologically important materials currently used in integrated circuits such as Si or GaAs.[3,4] Thus far, the spin of the carriers has played a minor role in semiconductor devices mainly because Si and GaAs are nonmagnetic. On the other hand, the enhanced spin-related phenomena realized in diluted magnetic semiconductors (DMS) (especially GaMnAs films[5]) open the way for applications in spintronics.[6−8] The successful demonstration of the injection of polarized spins in spintronic devices[9] involves Mn-doped DMS as spin injectors. However, such doping significantly affects their homogeneity[10,11] which may cause strong spin-flip scattering of spin-polarized carriers making spin injection rather ineffective.

Recent years witnessed many attempts to inject spin-polarized electrons into Si[4], but large currents with high spin polarization are yet to be demonstrated. Optical orientation of spins is inefficient in Si owing its indirect band gap. Perhaps the most promising strategy in creating spin-polarized carriers in conventional electronic devices is to integrate materials with high spin polarization with Si *by means of electrical contact*. Here one needs to find a way for (a) effective spin injection and (b) effective maintenance of spin polarization in the host material. Silicon has long been predicted a superior spintronic material for effective maintenance of spin polarization having exceptionally long spin coherence lifetime ($\sim 10^{-5}$–10^{-4} s) and spin-decoherence transport length ($\sim 1\ \mu$m) due to very weak spin–orbit interaction and lattice inversion symmetry.[12,13] In contrast, much work on metallic ferromagnetic (FM) spin injectors proved them to be ineffective in both ohmic regime and tunneling injection.[3,4,14] Perhaps the best choice for the FM injector in such devices is magnetic semiconductors (MS) because of their compatibility with nonmagnetic semiconductors: the use of MS as a spin-polarized carrier injector avoids the so-called "conductivity mismatch"[15] which presents a fundamental difficulty for effective spin injection into a semiconductor from the FM metals. Materials such as DMS Mn-doped Si,[16] Mn-doped chalcopyrites,[17] or MS EuO[18] have all been suggested, but none as yet have been demonstrated as a spin injector for Si.[19]

Being representatives of strongly correlated electron systems, MS demonstrate strong dependence of electrical and optical properties on the magnetization and spin fluctuations of their magnetic lattice.[20] Concentrated MS offer several important

Received: December 17, 2014
Accepted: February 27, 2015
Published: February 27, 2015

DOI: 10.1021/am5089007
ACS Appl. Mater. Interfaces 2015, 7, 6146–6152

advantages over DMS such as higher magnetization, spatial magnetic homogeneity, and wider range of conductivity tuning by doping, so that they can be used as spin filters in the insulating state and as spin injectors when doped.[21,22] Being doped, though, these materials typically enter into dominant states that are not spatially homogeneous due to formation of spin polarons.[20,23−26] However, this unwanted formation does not take place when magnetization of the lattice is significant, leaving the host material perfectly homogeneous in the region of its employment as a spin injector.[24−26]

Owing to its outstanding magnetic and transport properties among other MS, EuO has recently attracted much attention as having tremendous potential for semiconductor spintronics, in particular, when integrated with Si.[18,27−29] Not only does doped EuO exhibit a spin polarization close to 100% due to enormous (~0.6 eV) spin splitting of its conduction band but also it can be conductance-matched with Si by doping with oxygen vacancies or trivalent rare-earth atoms such as Gd, La, or Lu.[18,29−32] Its Heisenberg-like magnetism (7 μ_B per Eu^{2+} ion) arises from the half-filled 4f states which constitute the top of the valence band.[32] Stoichiometric EuO has a low FM Curie temperature T_c of about 69 K, but chemical doping and axial strain can increase T_c significantly.[31−35] Its band gap of 1.12 eV matches that of Si.[32] In addition to their structural compatibility, EuO is the only binary magnetic oxide that exhibits thermodynamic stability in contact with Si.[36] Its remarkable bulk properties—metal−insulator transition accompanied by 13−15 orders of magnitude change in resistivity, colossal magnetoresistivity effect of about 6 orders of magnitude in a modest magnetic field of 2 T, exceptionally strong magneto-optics effects, and a high sensitivity of transport and magnetic properties to doping[18,32] —plant firm expectation that the functionality of spin-selective ohmic EuO/Si devices[18] can be tuned as never before.

Despite the tremendous potential for spintronics, the epitaxial growth of single-crystalline stoichiometric EuO films *directly* on Si has not been reported to date.[27] Thin films of EuO can be epitaxially grown on inert substrates like $YAlO_3$,[37] yttria-stabilized cubic zirconia (YSZ),[38] graphene,[39] or MgO,[40] especially when the lattice mismatch is small, but stabilization of EuO on reactive surfaces of Si and GaAs[41] is notoriously difficult leading to polycrystalline EuO[27,37] and/or weak or no FM behavior.[41] The breakthrough for integration of EuO with Si has been achieved by using an intermediate SrO buffer layer.[18,42] An intermediate layer, however, reduces the probability of spin-polarized carriers injection exponentially.

The continuing attempts to grow EuO/Si heterojunctions[27−29,43,44] are checked by the presence of large amounts of impurity phases at the interface. These phases are not only detrimental to the growth of EuO films, but they also prevent spin injection. Thus, in order to create functional structures in which the properties of the underlying silicon and the overlying EuO film both attain their full potential, there is a clear need for direct *epitaxial* growth making an *ohmic* contact between EuO and Si.

Here we report specific methods that make possible a direct epitaxial integration of stoichiometric single-crystalline EuO films with Si. The structural and magnetic properties of our films rival those of bulk single crystals. We show that the control of the silicon/oxide interface is critical for the direct epitaxial growth and specific preparation of Si surface allows implementation of such control. In addition, we solve the technological problem of a capping layer for EuO films by controlled formation of a very thin (~2−3 nm) layer of Eu_2O_3 on the surface, which prevents further oxidation and/or hydration pretty much the same way as Al_2O_3 layer protects Al metal.

EXPERIMENTAL SECTION

Thin films of EuO have been grown by molecular beam epitaxy (MBE) in Riber Compact 12 system modified for the growth of oxides. The background pressure is less than 10^{-10} Torr. Eu (99.99% purity), O_2 (99.9995% purity), SiO_x (99.99% purity), and Al (99.999% purity) were used as precursors. All materials were evaporated from BN effusion cells. High-ohmic Si(001) wafers with 0.5° miscut angle were used as substrates. Cell and substrate temperatures were measured by thermocouples. Approximate cell temperatures were T_{Eu} ~ 500 °C, T_{SiOx} ~ 950 °C, and T_{Al} ~ 950 °C. Substrate temperatures above 270 °C were also controlled by an optical infrared pyrometer with the working wavelength 0.9 μm. Reflection high-energy electron diffraction (RHEED) was used for in situ control of the crystalline and morphological state of the surface. The measurements were made with use of kSA 400 RHEED system, k-Space Associates, Inc. Fluxes of all the reactants were meticulously controlled by hot cathode beam flux monitor. Oxygen pressure was also monitored in situ by mass spectrometer.

Magnetic measurements were performed with SQUID Quantum Design MPMS XL-7. X-ray diffraction spectra were recorded with use of Bruker K8 Advance and Rigaku SmartLab 9 kW spectrometers with CuKα radiation. Rutherford backscattering spectra were measured for He ions with the energy 1.7 MeV.

RESULTS AND DISCUSSION

Interfacing EuO with silicon is a major challenge: in addition to the significant thermal and enormous (+5.6%) lattice mismatch, it adds the complexity of joining covalent systems to ionic ones, chemical interactions at interfaces, and possible compositional and structural changes. That is why we had a long way to go to grow epitaxial films of EuO directly on Si. Our first attempts followed a standard route for EuO growth. Adsorption controlled (distillation) regime is suitable for formation of high-quality EuO films on oxide substrates ($YAlO_3$, YSZ, MgO, etc.). The term "distillation" is commonly used[27,28,38,39] to describe the EuO growth mode based on larger than stoichiometric Eu flux to prevent formation of higher oxides, with excessive Eu atoms being evaporated. The latter process requires high substrate temperatures (above 400 °C). Exposure of Si substrate to high temperature, though, leads to formation of amorphous SiO_2 and metal bulk silicide $EuSi_2$ in oxidizing and reducing environment, respectively. These reactions are suppressed at lower temperatures, but any departure from stoichiometry boosts formation of higher oxides (Eu_3O_4 and/or Eu_2O_3) or large number of vacancies (EuO_{1-x}). As a result, the range of the temperatures and ratios of Eu and O_2 fluxes is extremely narrow, making selection of optimal growth parameters notoriously difficult. Obviously, Si surface calls for protection.

The seminal paper by McKee et al.[45] has provided a robust solution to the long-standing problem of growing a commensurate single-crystalline oxide interface with Si by employing intermediate submonolayer alkaline-earth silicide (the number of metal atoms is less than the number of surface Si atoms) to protect the silicon surface from oxidation. The clean unreconstructed (100) silicon surface is formed by Si atoms with two singly occupied dangling bonds per atom. Pairs of silicon atoms form covalent chemical bonds leading to the dimer row (2 × 1) reconstruction, which consists of alternating (2 × 1) and (1 × 2) domains separated by single-atom height

DOI: 10.1021/am5089007
ACS Appl. Mater. Interfaces 2015, 7, 6146−6152

steps. It leaves one singly occupied dangling bond per atom making silicon surface highly reactive. Formation of surface alkaline-earth silicide is aimed at the saturation of these dangling bonds to exploit reactivity of the Si surface in a controlled fashion. Most of the studies involve strontium which is highly relevant to the growth of EuO because almost identical ionic radii of Eu^{2+} and Sr^{2+} lead to the well-known isomorphism of Eu(II) and Sr compounds with very close structural parameters.

The standard procedure for Sr-passivation of the Si surface includes creation of Sr adlayer with the coverage of 1/2 monolayer (ML) corresponding to the stoichiometry $SrSi_2$. Each metal atom donates two electrons, and, therefore, each dangling bond becomes occupied by an electron pair. As a result, this structure has no surface states in the band gap of the host,[46] which is rather important for applications. The presence of a band gap adds to the resistance of the surface to oxidation.[47] Such (1×2) reconstruction is routinely used for the growth of AO and ABO_3 compounds on Si, including EuO.[18,29,42] However, both our results and other reports show the presence of impurity phases in such EuO/Si structures. It means that the protection of the surface is not sufficient for producing clean EuO/Si interface and other options should be explored.

It is known that adsorption of Sr (and similarly Eu) on the (100) silicon surface results in a phase diagram which involves a series of surface reconstructions depending on the temperature and the metal coverage—they can be used in an attempt to improve the surface protection. The (2×3) structure[48] corresponding to 1/6 ML metal coverage has a large amount of unsaturated dangling bonds, and it is almost as reactive as pure Si. Indeed, an attempt to use this structure as a template for BaO leads to an amorphous growth.[49] Both our results and the literature data[49] indicate that low- and high-temperature procedures to obtain the (1×2) reconstruction of the surface are very similar as long as the quality of the grown oxide is concerned.

Better results are expected from surface silicides with higher than 1/2 ML metal coverage of the surface. Our experiments show that Eu forms a stable surface silicide with the (1×5) reconstruction. Similar reconstructions have been detected for other divalent metals Yb, Ca, and Sr,[50−52] but their atomic structure and the stoichiometry are debated. Higher metal coverage should provide better protection of the surface. What is most important is that it does not lead to surface states in the band gap of silicon because the structure is expected to be formed by breaking Si−Si dimers and saturating the resulting free valences with metal atoms. This can be confirmed by electron spin resonance (ESR) measurements which proved to be extremely sensitive to the presence of unpaired electrons (dangling chemical bonds). Indeed, we do not observe any ESR signal for Si protected by surface europium silicide for both structures with (1×2) and (1×5) reconstructions. According to different models of oxide growth (see, for example, ref 46) metal atoms in the surface silicide form bonds with oxygen atoms and, therefore, become incorporated into the oxide subsystem. Oxidation of M−Si bonds and formation of M−O−Si structures are supported by a number of experiments.[51,53] In this sense the surface silicide is not a buffer of submonolayer thickness but a natural precursor to the Si/oxide interface.

The conclusion about better protection of the surface by silicides with higher metal content has some experimental backing: the authors of ref 51 mention that among four different reconstructions of Ba and Sr on silicon used to grow lattice-matched $Ba_{0.7}Sr_{0.3}O$, the best results are obtained for the (1×5) reconstruction of Sr on Si. Although this result cannot be directly transferred to the growth of EuO on Si due to the large lattice mismatch and high reactivity of EuO, it is a strong indication that the use of the (1×5) reconstruction may add crucial advantages to the growth process. It is likely that the excessive relatively loosely bound metal atoms intercept molecular and atomic oxygen species, the latter being the main cause of the Si surface degradation. It is quite similar to the common protection recipe based on the cover of the surface silicide by an additional layer of physisorbed metal at low temperature.[45] Our results below show that this improved protection of the Si surface leads to direct epitaxial integration of EuO with silicon.

To remove the natural amorphous SiO_2 layer, substrates were heated up to 950 °C where SiO_2 is volatile. The resulting RHEED pattern clearly demonstrates formation of the Si $(2 \times 1) + (1 \times 2)$ reconstruction−dimerization of surface Si atoms. The resulting Si surface has been also studied with Auger spectroscopy for traces of carbon at the surface. Experiments with increased sensitivity, attempting to register peaks at 270 eV, do not detect any signals from carbon. To form a protective submonolayer Eu silicide, the reconstructed bare Si surface is exposed to Eu flux at the temperature 660 °C. The increasing Eu coverage leads to a series of surface phases as witnessed by RHEED: $(2 \times 1) + (1 \times 2)$ Si reconstruction is transformed into $(2 \times 3) + (3 \times 2)$, then into $(1 \times 2) + (2 \times 1)$, and finally into $(1 \times 5) + (5 \times 1)$ (Figure 1). Periodic symmetries $(m \times n)$ and $(n \times m)$ are both present for surfaces with steps of single-atom height. The sequence of transformations is the following: (2×1) Si into (2×3), (1×2), and then into (1×5) silicide phase. The resulting state of the surface depends on the fine balance of Eu adsorption and desorption, which can be tuned by substrate temperature and Eu flux. Formation of Eu on Si structure with $(1 \times 5) + (5 \times 1)$ reconstruction takes approximately half a minute for the Eu flux of about 5×10^{-8} Torr. The resulting surface silicide phase remains stable at lower temperatures.

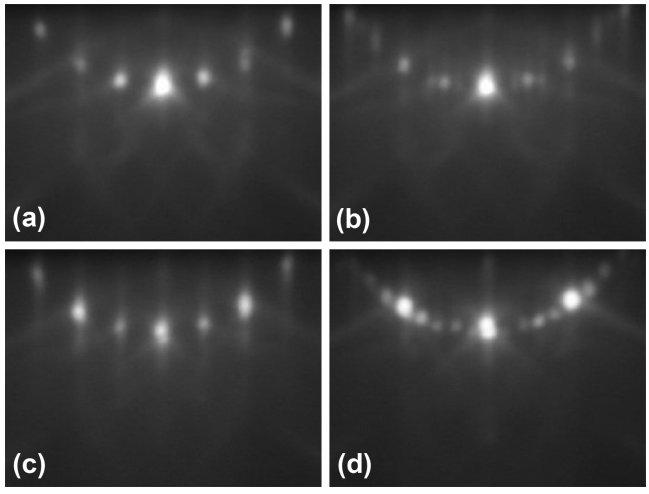

Figure 1. RHEED images along the [110] azimuth of reconstructed surface phases: (a) $(2 \times 1) + (1 \times 2)$ Si; (b) $(2 \times 3) + (3 \times 2)$ Eu on Si; (c) $(1 \times 2) + (2 \times 1)$ Eu on Si; (d) $(1 \times 5) + (5 \times 1)$ Eu on Si.

To grow thin EuO films on thus-protected Si surfaces, we developed a two-step protocol. The first step is a low-

DOI: 10.1021/am5089007
ACS Appl. Mater. Interfaces 2015, 7, 6146−6152

temperature growth (stage A) in close to stoichiometric regime with slight excess of Eu atoms to avoid formation of SiO_2 and bulk $EuSi_2$. It may seem counterintuitive that formation of $EuSi_2$ is avoided by an excess of Eu flux. The reason is that the protected Si surface is stable with respect to a mild flux of Eu but quickly degrades when exposed to oxygen. Thus, the bulk $EuSi_2$ does not form at the interface unless the integrity of the surface is destroyed by oxygen.

The low-temperature EuO growth starts with simultaneous supply of Eu and oxygen. The EuO film stoichiometry requires fine-tuning of the substrate temperature and fluxes. It was performed step by step on the basis of approximate hot cathode beam flux monitor values, with further directions provided by RHEED patterns. For a successful growth, we use Eu flux in the range from 2×10^{15} to 2×10^{16} atoms cm^{-2} min^{-1} and the oxygen pressure from 5×10^{-9} to 2×10^{-8} Torr. The substrate temperature has been varied from 350 to 370 °C. We find that 10 MLs of EuO are enough to prevent formation of unwanted phases. One monolayer of EuO is defined as a single Eu−O plane; i.e., it corresponds to half of the lattice parameter in the direction normal to the surface. The growth rate is estimated by dividing the thickness of relatively thick films by the time of their growth. The grown 10 ML film is stable up to 510 °C at least, and it is annealed at that temperature for 15 min to improve the crystalline quality. The RHEED image at the end of this procedure is shown in Supporting Information Figure 1. The XRD-pattern of the same sample capped by SiO_x for ex situ studies is shown in Supporting Information Figure 2. Results of magnetic measurements are presented in Supporting Information Figure 3. At high temperature the Si diffusion into the film may lead to its amorphization. Our experiments show that such process occurs above 550 °C (for comparison, the BaO/Si junction remains crystalline after being kept at 500 °C but becomes amorphous at 580 °C).[54] Annealing of ultrathin EuO films at about 500 °C does not lead to deterioration of their magnetic properties.

Changes of the EuO lateral lattice parameter during EuO growth can be determined from the evolution of the distance between streaks in corresponding RHEED patterns. Figure 2

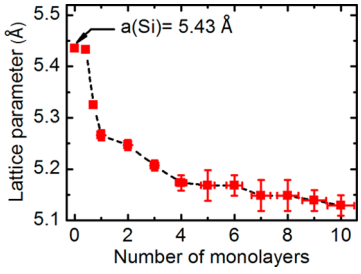

Figure 2. Changes of the lateral lattice parameter at the low temperature (stage A) of EuO growth as determined by distance between reflections in the RHEED pattern. After growth of 10 MLs the film is completely relaxed. XRD measurements of thick EuO films also show that the vertical lattice parameter is very close to the bulk value.

shows that highly stretched layers of EuO become progressively more relaxed and the lattice parameter changes from the value corresponding to Si (5.43 Å) toward that of bulk EuO (5.14 Å). The changes are not uniform: the first 4 MLs exhibit the largest lattice relaxation; 10 MLs of EuO on Si guarantee the full lattice relaxation. Because of considerable lattice mismatch of EuO and Si, one expects growth of 3D islands, followed by pseudomorphic growth, which are typical for the Stranski−Krastanov regime. Instead, we do not see any form of 3D growth—the intensity of RHEED reflections is modulated rather slightly along the streaks, but, what is most important, typical spots characteristic to 3D growth are not detected.

The second step (stage B) is the growth at higher temperature (470 °C), where it is controlled by Eu distillation. The rate of the growth is kept at about 40 nm/h. This step is similar to the growth of EuO on oxide substrates. The following annealing at 530 °C is aimed at improvement of crystalline quality and decrease of the number of point defects. Typical RHEED image of EuO film grown this way is shown in Figure 3 and consists of streaks, indicating that the surface is smooth.

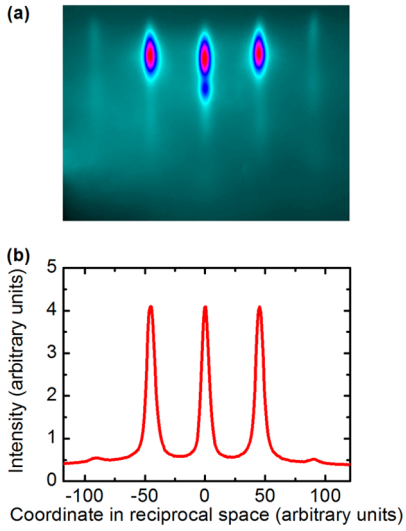

Figure 3. (a) Typical RHEED image along the [110] azimuth of the fully (according to the two-step protocol) grown d_{EuO} = 40 nm thick EuO film; (b) corresponding horizontal intensity profile.

Observation of clean and sharp Kikuchi lines is also characteristic of a perfect crystal. It is most important that the proposed recipe yields *stable reproducible results*: grown films have identical properties. One can notice that the two-step procedure is reminiscent of growth of EuO on Si with protective buffer layer of SrO. The important difference is that in our case EuO is grown in direct contact with Si making efficient spin injection possible.

EuO is highly reactive and when exposed to the atmosphere it forms hydroxide, higher oxides, and even carbonate. Degradation of unprotected EuO thin films is very fast. Different materials have been proposed and used as capping layers: Si, Ti, Al, SiO_x, Al_2O_3, etc. Our experiments show that thick enough capping layers formed at room temperature by Al and SiO_x evaporated from effusion cells provide sufficient protection. We propose a more advanced way to protect EuO films without introducing new components to the system. It is based on *controlled* oxidation of the surface of EuO with formation of inert Eu_2O_3. EuO films were exposed to a low oxygen flux (5×10^{-8} Torr) in the vacuum chamber. The initially bright RHEED pattern extinguishes so that EuO reflections, although strongly obscured, are still visible. EuO films protected by Eu_2O_3 layer show no signs of degradation after months-long exposure to the air: both X-ray diffraction pattern and visual appearance remain unchanged. X-ray

DOI: 10.1021/am5089007
ACS Appl. Mater. Interfaces 2015, 7, 6146−6152

reflectivity measurements estimate the thickness of the protective layer to be about 2−3 nm.

X-ray diffraction measurements of EuO films are shown in Figure 4. In contrast to other works, our $\theta-2\theta$ diffraction scan

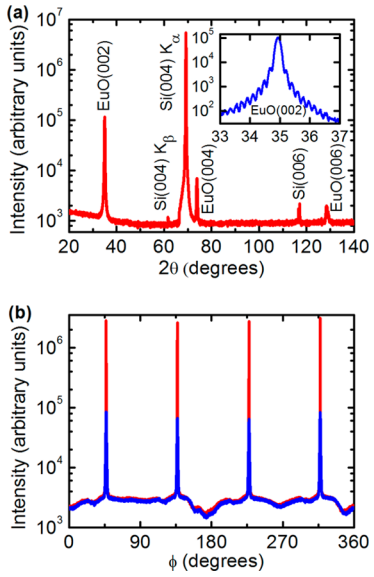

Figure 4. X-ray diffraction scans of SiO_x/EuO/Si sample (d_{EuO} = 40 nm): (a) $\theta-2\theta$ diffraction spectrum; inset: thickness fringes of EuO (002) peak; (b) φ-scans of reflections for EuO(202) (blue) and Si(202) (red).

(Figure 4a) demonstrates peaks from (002), (004), and (006) reflections without any traces of unwanted phases. All the peaks correspond to the same orientation of EuO and Si atomic planes. Maximal intensities of EuO(00n) and Si(00n) XRD reflections are observed for the same orientation of the sample, demonstrating that the angle between lateral atomic planes is negligible. Location of EuO reflections in the $\theta-2\theta$ diffraction pattern corresponds to the lattice parameter a = 5.1393 ± 0.0001 Å, which is very close to the bulk value (5.1435 Å). Significant tetragonal distortions expected from elastic strains at the pseudomorphic growth are not detected. Full coincidence of EuO and Si peaks on (202) reflection φ-scan (Figure 4b) indicates that vertical facets of fcc structures of both systems are also aligned in parallel. Hence, the grown EuO films are epitaxial. Well-developed thickness fringes are observed for the EuO(002), EuO(004), and EuO(006) reflections. The inset of Figure 4a shows them for the EuO(002) reflection. This characteristic feature of the X-ray diffraction is a result of the wave interference due to reflections at the interfaces, both top and bottom. Taking into account the value of the X-ray wavelength (1.5418 Å), the observation of the thickness fringes is a fingerprint of sharp interfaces; otherwise, the reflected waves cannot maintain the coherence and thickness fringes would not show up.

The stoichiometry of the grown EuO films was controlled by Rutherford backscattering (RBS). A characteristic RBS spectrum of the EuO films is shown in Supporting Information Figure 4. The best fit corresponds to stoichiometric EuO. The calculated thickness of the films corresponds perfectly to the values determined from the periods of XRD thickness fringes. RBS spectra exhibit strong channeling—yet another indication of the epitaxial integration of EuO and Si. It is evident from the spectra that the amplitude of the Eu peak diminishes when the incident ion beam is aligned along the [001] axis of the Si substrate.

Magnetic measurements (using superconducting quantum interference device) of both the fully grown EuO films (stages A and B) and the first low-temperature 10 MLs (stage A) exhibit the onset of ferromagnetism. Figure 5a shows

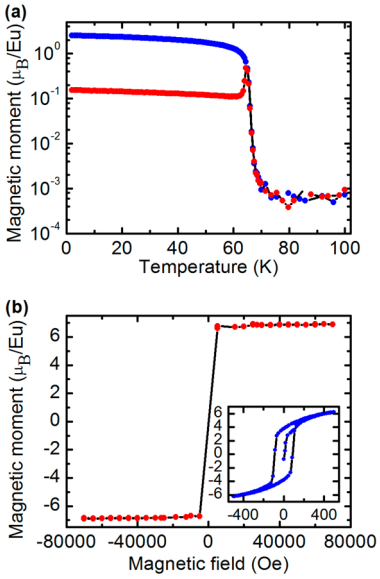

Figure 5. (a) Temperature dependences of the dc magnetization of epitaxial SiO_x/EuO/Si heterostructure (d_{EuO} = 40 nm) for two cases: warm-up after cooling in zero field (red) and cooling after warming in the field (blue), both recorded for magnetic field H = 1 Oe applied parallel to the film surface. (b) In-plane magnetization of epitaxial EuO film on Si as a function of the applied magnetic field $H\|[100]$ at T = 2 K. Inset shows hysteresis loop.

temperature dependence of the in-plane dc magnetization of the fully grown EuO film in external magnetic field H = 1 Oe. Temperature dependence of the ac (1 Hz frequency) magnetic susceptibility of the same EuO film in external magnetic field H = 0 is presented in Figure 6. The Curie temperature is

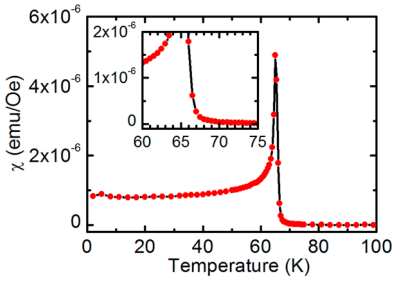

Figure 6. Temperature dependence of the ac (1 Hz) magnetic susceptibility of epitaxial SiO_x/EuO/Si structure (d_{EuO} = 40 nm) in zero external magnetic field.

determined from both dc and ac measurements to amount 68 ± 1 K—the same as in the bulk EuO. Any significant amount of defects would shift T_c above the error bars. (The perfect stoichiometry also makes our EuO films highly insulating, which prevents conventional measurements of their transport properties due to shunting by Si substrate.) The field dependence of in-plane dc magnetization measured at 2 K (inset of Figure 5b) shows hysteresis with coercivity ~90 Oe.

DOI: 10.1021/am5089007
ACS Appl. Mater. Interfaces 2015, 7, 6146−6152

The saturation magnetization (Figure 5b) per Eu atom is determined to be 6.9 ± 0.1 μ_B. This is consistent with the best bulk samples and corresponds to $4f^7$ configuration of Eu^{2+}.

Ten-monolayer-thick films show somewhat decreased temperature of the ferromagnetic transition (see Supporting Information Figure 3). This is not that surprising as spontaneous magnetization of the Heisenberg ferromagnet EuO is caused by interatomic exchange interaction which strongly depends on the distance between Eu ions. Our RHEED measurements of the lattice parameter changes during stage A of the growth clearly show that EuO is laterally stretched (Figure 2). As a consequence, Eu−Eu distances become larger, and, hence, the Curie temperature becomes smaller than in the bulk. The magnetic measurements of these ultrathin films show no reduction of the magnetic moment per Eu atom. In combination with RHEED in situ control of the surface at the growth, the observed channeling in the RBS spectra, and φ-scans of XRD reflections, it makes us confident that we indeed achieved an *epitaxial* growth of EuO directly on Si without any significant inclusions of unwanted phases at the interface.

CONCLUSION

In summary, we provide a recipe for epitaxial integration of EuO directly with silicon, which may have general implications for the growth of functional oxides. We believe that there are two key ingredients, which made the solution possible. First is the protection of the Si surface with the surface silicide having a larger metal content; in our case it corresponds to (1 × 5) reconstruction. Clearly, this recipe is not limited to europium silicide and the growth of EuO; it can be used for protection of the Si surface by strontium silicide and improved growth of other oxide materials, including complex ones. Second, the developed two-step growth protocol with the low-temperature stoichiometric regime preceding the adsorption-controlled growth ensures sharp and uniform interfaces without any impurity phases being detected. The proposed procedure of EuO protection by a layer of Eu_2O_3 seems to be clean and easy to implement. The grown thin films of EuO thus become ideal candidates for successful injection of spin-polarized electrons into Si. We are currently exploring this possibility—the results will be published elsewhere. We hope that our studies open up a viable route to the ultimate goals of semiconductor spintronics.

ASSOCIATED CONTENT

Supporting Information

Properties of EuO layers after stage A: RHEED, XRD, magnetization measurements; RBS spectra of Eu_2O_3/EuO/Si heterostructure. This material is available free of charge via the Internet at http://pubs.acs.org.

AUTHOR INFORMATION

Corresponding Author

*E-mail: mussr@triumf.ca.

Author Contributions

The manuscript was written through contributions of all authors. All authors have given approval to the final version of the manuscript.

Notes

The authors declare no competing financial interest.

ACKNOWLEDGMENTS

The authors are grateful to O. E. Parfenov for discussions and to S. V. Gudenko for ESR measurements. The work is financially supported by NRC "Kurchatov Institute", Russian Foundation for Basic Research through grant 13-07-00095, and Russian Science Foundation through grant 14-19-00062.

REFERENCES

(1) Prinz, G. A. Magnetoelectronics. *Science* **1998**, *282*, 1660−1663.
(2) Wolf, S. A.; Awschalom, D. D.; Buhrman, R. A.; Daughton, J. M.; von Molnár, S.; Roukes, M. L.; Chtchelkanova, A. Y.; Treger, D. M. Spintronics: A Spin-Based Electronics Vision for the Future. *Science* **2001**, *294*, 1488−1495.
(3) Awschalom, D. D.; Flatté, M. E. Challenges for Semiconductor Spintronics. *Nat. Phys.* **2007**, *3*, 153−159.
(4) Jansen, R. Silicon Spintronics. *Nat. Mater.* **2012**, *11*, 400−408.
(5) Ohno, H.; Shen, A.; Matsukura, F.; Oiwa, A.; Endo, A.; Katsumoto, S.; Iye, Y. (Ga,Mn)As: A New Diluted Magnetic Semiconductor Based on GaAs. *Appl. Phys. Lett.* **1996**, *69*, 363−365.
(6) Ohno, H. Making Nonmagnetic Semiconductors Ferromagnetic. *Science* **1998**, *281*, 951−956.
(7) Ohno, H.; Chiba, D.; Matsukura, F.; Omiya, T.; Abe, E.; Dietl, T.; Ohno, Y.; Ohtani, K. Electric-Field Control of Ferromagnetism. *Nature* **2000**, *408*, 944−946.
(8) Tang, H. X.; Kawakami, R. K.; Awschalom, D. D.; Roukes, M. L. Giant Planar Hall Effect in Epitaxial (Ga,Mn)As Devices. *Phys. Rev. Lett.* **2003**, *90*, 107201.
(9) Ohno, Y.; Young, D. K.; Beschoten, B.; Matsukura, F.; Ohno, H.; Awschalom, D. D. Electrical Spin Injection in a Ferromagnetic Semiconductor Heterostructure. *Nature* **1999**, *402*, 790−792.
(10) Jungwirth, T.; Sinova, J.; Mašek, J.; Kučera, J.; MacDonald, A. H. Theory of Ferromagnetic (III,Mn)V Semiconductors. *Rev. Mod. Phys.* **2006**, *78*, 809−864.
(11) Storchak, V. G.; Eshchenko, D. G.; Morenzoni, E.; Prokscha, Th.; Suter, A.; Liu, X.; Furdyna, J. K. Spatially Resolved Inhomogeneous Ferromagnetism in (Ga,Mn)As Diluted Magnetic Semiconductors: A Microscopic Study by Muon Spin Relaxation. *Phys. Rev. Lett.* **2008**, *101*, 027202.
(12) Žutić, I.; Fabian, J.; Das Sarma, S. Spintronics: Fundamentals and Applications. *Rev. Mod. Phys.* **2004**, *76*, 323−410.
(13) Appelbaum, I.; Huang, B.; Monsma, D. J. Electronic Measurement and Control of Spin Transport in Silicon. *Nature* **2007**, *447*, 295−298.
(14) Hammar, P. R.; Bennett, B. R.; Yang, M. J.; Johnson, M. Observation of Spin Injection at a Ferromagnet−Semiconductor Interface. *Phys. Rev. Lett.* **1999**, *83*, 203−206.
(15) Schmidt, G.; Ferrand, D.; Molenkamp, L. W.; Filip, A. T.; van Wees, B. J. Fundamental Obstacle for Electrical Spin Injection from a Ferromagnetic Metal into a Diffusive Semiconductor. *Phys. Rev. B* **2000**, *62*, R4790−R4793.
(16) Bolduc, M.; Awo-Affouda, C.; Stollenwerk, A.; Huang, M. B.; Ramos, F. G.; Agnello, G.; LaBella, V. P. Above Room Temperature Ferromagnetism in Mn-Ion Implanted Si. *Phys. Rev. B* **2005**, *71*, 033302.
(17) Erwin, S. C.; Žutić, I. Tailoring Ferromagnetic Chalcopyrites. *Nat. Mater.* **2004**, *3*, 410−414.
(18) Schmehl, A.; Vaithyanathan, V.; Herrnberger, A.; Thiel, S.; Richter, Ch.; Liberati, M.; Heeg, T.; Röckerath, M.; Kourkoutis, L. F.; Mühlbauer, S.; Böni, P.; Muller, D. A.; Barash, Y.; Schubert, J.; Idzerda, Y.; Mannhart, J.; Schlom, D. G. Epitaxial Integration of the Highly Spin-Polarized Ferromagnetic Semiconductor EuO with Silicon and GaN. *Nat. Mater.* **2007**, *6*, 882−887.
(19) Appelbaum, I. Introduction to Spin-Polarized Ballistic Hot Electron Injection and Detection in Silicon. *Philos. Trans. R. Soc. London, Ser. A* **2011**, *369*, 3554−3574.
(20) Coey, J. M. D.; Viret, M.; von Molnár, S. Mixed-Valence Manganites. *Adv. Phys.* **1999**, *48*, 167−293.

DOI: 10.1021/am5089007
ACS Appl. Mater. Interfaces 2015, 7, 6146−6152

(21) Santos, T. S.; Moodera, J. S. Observation of Spin Filtering with a Ferromagnetic EuO Tunnel Barrier. *Phys. Rev. B* **2004**, *69*, 241203(R).
(22) Trbovic, J.; Ren, C.; Xiong, P.; von Molnár, S. Spontaneous Spin-Filter Effect across EuS/GaAs Heterojunction. *Appl. Phys. Lett.* **2005**, *87*, 082101.
(23) von Molnár, S.; Stampe, P. A. In *Handbook of Magnetism and Advanced Magnetic Materials*; Kronmueller, H., Parkin, S., Eds.; Wiley: New York, 2007; Vol. *5*.
(24) Storchak, V. G.; Parfenov, O. E.; Brewer, J. H.; Russo, P. L.; Stubbs, S. L.; Lichti, R. L.; Eshchenko, D. G.; Morenzoni, E.; Aminov, T. G.; Zlomanov, V. P.; Vinokurov, A. A.; Kallaher, R. L.; von Molnár, S. Direct Observation of Magnetic Polaron. *Phys. Rev. B* **2009**, *80*, 235203.
(25) Storchak, V. G.; Parfenov, O. E.; Brewer, J. H.; Russo, P. L.; Stubbs, S. L.; Lichti, R. L.; Eshchenko, D. G.; Morenzoni, E.; Zlomanov, V. P.; Vinokurov, A. A.; Bamburov, V. G. Novel Muonium Centers—Magnetic Polarons—in Magnetic Semiconductors. *Physica B* **2009**, *404*, 899−902.
(26) Storchak, V. G.; Eshchenko, D. G.; Morenzoni, E.; Ingle, N.; Heiss, W.; Schwarzl, T.; Springholz, G.; Kallaher, R. L.; von Molnár, S. Magnetic Polarons in Eu-Based Films of Magnetic Semiconductors. *Phys. Rev. B* **2010**, *81*, 153201.
(27) Caspers, C.; Müller, M.; Gray, A. X.; Kaiser, A. M.; Gloskovskii, A.; Fadley, C. S.; Drube, W.; Schneider, C. M. Chemical Stability of the Magnetic Oxide EuO Directly on Silicon Observed by Hard X-ray Photoemission Spectroscopy. *Phys. Rev. B* **2011**, *84*, 205217.
(28) Caspers, C.; Flade, S.; Gorgoi, M.; Gloskovskii, A.; Drube, W.; Schneider, C. M.; Müller, M. Ultrathin Magnetic Oxide EuO Films on Si(001) Using SiO_x Passivation—Controlled by Hard X-Ray Photoemission Spectroscopy. *J. Appl. Phys.* **2013**, *113*, 17C505.
(29) Mundy, J. A.; Hodash, D.; Melville, A. J.; Held, R.; Mairoser, T.; Muller, D. A.; Kourkoutis, L. F.; Schmehl, A.; Schlom, D. G. Hetero-Epitaxial EuO Interfaces Studied by Analytic Electron Microscopy. *Appl. Phys. Lett.* **2014**, *104*, 091601.
(30) Steeneken, P. G.; Tjeng, L. H.; Elfimov, I.; Sawatzky, G. A.; Ghiringhelli, G.; Brookes, N. B.; Huang, D.-J. Exchange Splitting and Charge Carrier Spin Polarization in EuO. *Phys. Rev. Lett.* **2002**, *88*, 047201.
(31) Ingle, N. J. C.; Elfimov, I. S. Influence of Epitaxial Strain on the Ferromagnetic Semiconductor EuO: First-Principles Calculations. *Phys. Rev. B* **2008**, *77*, 121202(R).
(32) Mauger, A.; Godart, C. The Magnetic, Optical, and Transport Properties of Representatives of a Class of Magnetic Semiconductors: The Europium Chalcogenides. *Phys. Rep.* **1986**, *141*, 51−176.
(33) Mairoser, T.; Schmehl, A.; Melville, A.; Heeg, T.; Canella, L.; Böni, P.; Zander, W.; Schubert, J.; Shai, D. E.; Monkman, E. J.; Shen, K. M.; Schlom, D. G.; Mannhart, J. Is There an Intrinsic Limit to the Charge-Carrier-Induced Increase of the Curie Temperature of EuO? *Phys. Rev. Lett.* **2010**, *105*, 257206.
(34) Mairoser, T.; Loder, F.; Melville, A.; Schlom, D. G.; Schmehl, A. Influence of Chemical Doping on the Magnetic Properties of EuO. *Phys. Rev. B* **2013**, *87*, 014416.
(35) Melville, A.; Mairoser, T.; Schmehl, A.; Birol, T.; Heeg, T.; Holländer, B.; Schubert, J.; Fennie, C. J.; Schlom, D. G. Effect of Film Thickness and Biaxial Strain on the Curie Temperature of EuO. *Appl. Phys. Lett.* **2013**, *102*, 062404.
(36) Hubbard, K. J.; Schlom, D. G. Thermodynamic Stability of Binary Oxides in Contact with Silicon. *J. Mater. Res.* **1996**, *11*, 2757−2776.
(37) Beukers, J. N.; Kleibeuker, J. E.; Koster, G.; Blank, D. H. A.; Rijnders, G.; Hilgenkamp, H.; Brinkman, A. Epitaxial EuO Films by Pulsed Laser Deposition Monitored by in Situ X-ray Photoelectron Spectroscopy. *Thin Solid Films* **2010**, *518*, 5173−5176.
(38) Sutarto, R.; Altendorf, S. G.; Coloru, B.; Moretti Sala, M.; Haupricht, T.; Chang, C. F.; Hu, Z.; Schüßler-Langeheine, C.; Hollmann, N.; Kierspel, H.; Hsieh, H. H.; Lin, H.-J.; Chen, C. T.; Tjeng, L. H. Epitaxial and Layer-by-Layer Growth of EuO Films on Yttria-Stabilized Cubic Zirconia (001) Using MBE Distillation. *Phys. Rev. B* **2009**, *79*, 205318.
(39) Klinkhammer, J.; Förster, D. F.; Schumacher, S.; Oepen, H. P.; Michely, Th.; Busse, C. Structure and Magnetic Properties of Ultrathin Textured EuO Films on Graphene. *Appl. Phys. Lett.* **2013**, *103*, 131601.
(40) Iwata, N.; Pindoria, G.; Morishita, T.; Kohn, K. Preparation and Magnetic Properties of EuO Thin Films Epitaxially Grown on MgO and $SrTiO_3$ Substrates. *J. Phys. Soc. Jpn.* **2000**, *69*, 230−236.
(41) Swartz, A. G.; Ciraldo, J.; Wong, J. J. I.; Li, Y.; Han, W.; Lin, T.; Mack, S.; Shi, J.; Awschalom, D. D.; Kawakami, R. K. Epitaxial EuO Thin Films on GaAs. *Appl. Phys. Lett.* **2010**, *97*, 112509.
(42) Lettieri, J.; Vaithyanathan, V.; Eah, S. K.; Stephens, J.; Sih, V.; Awschalom, D. D.; Levy, J.; Schlom, D. G. Epitaxial Growth and Magnetic Properties of EuO on (001)Si by Molecular-Beam Epitaxy. *Appl. Phys. Lett.* **2003**, *83*, 975−977.
(43) Panguluri, R. P.; Santos, T. S.; Negusse, E.; Dvorak, J.; Idzerda, Y.; Moodera, J. S.; Nadgorny, B. Half-Metallicity in Europium Oxide Conductively Matched with Silicon. *Phys. Rev. B* **2008**, *78*, 125307.
(44) Wang, X.; Liu, P.; Fox, K. A.; Tang, J.; Colón Santana, J. A.; Belashchenko, K.; Dowben, P. A.; Sui, Y. Effects of Gd Doping and Oxygen Vacancies on the Properties of EuO Films Prepared via Pulsed Laser Deposition. *IEEE Trans. Magn.* **2010**, *46*, 1879−1882.
(45) McKee, R. A.; Walker, F. J.; Chisholm, M. Crystalline Oxides on Si: The First Five Monolayers. *Phys. Rev. Lett.* **1998**, *81*, 3014−3017.
(46) Först, C.; Ashman, C.; Schwarz, K.; Blöchl, P. The Interface between Silicon and a High-*k* Oxide. *Nature* **2003**, *427*, 53−56.
(47) Liang, Y.; Gan, C.; Engelhard, M. First Step Towards the Growth of Single-Crystal Oxides on Si: Formation of a Two-Dimensional Crystalline Silicate on Si(001). *Appl. Phys. Lett.* **2001**, *79*, 3591−3593.
(48) Kuzmin, M.; Perälä, R. E.; Laukkanen, P.; Väyrynen, I. J. Atomic Geometry and Electronic Structure of the Si(100) 2 × 3-Eu Surface Phase. *Phys. Rev. B* **2005**, *72*, 085343.
(49) Reiner, J. W.; Garrity, K. F.; Walker, F. J.; Ismail-Beigi, S.; Ahn, C. H. Role of Strontium in Oxide Epitaxy on Silicon (001). *Phys. Rev. Lett.* **2008**, *101*, 105503.
(50) Fan, W. C.; Wu, N. J.; Ignatiev, A. Observation of Ordered Structures of Sr on the Si(100) Surface. *Phys. Rev. B* **1990**, *42*, 1254−1257.
(51) Zachariae, J.; Pfnür, H. Growth Conditions, Stoichiometry, and Electronic Structure of Lattice-Matched SrO/BaO Mixtures on Si(100). *Phys. Rev. B* **2005**, *72*, 075410.
(52) Hu, X.; Yu, Z.; Curless, J. A.; Droopad, R.; Eisenbeiser, K.; Edwards, J. L., Jr.; Ooms, W. J.; Sarid, D. Comparative Study of Sr and Ba Adsorption on Si(100). *Appl. Surf. Sci.* **2001**, *181*, 103−110.
(53) Segal, Y.; Reiner, J. W.; Kolpak, A. M.; Zhang, Z.; Ismail-Beigi, S.; Ahn, C. H.; Walker, F. J. Atomic Structure of the Epitaxial BaO/Si(001) Interface. *Phys. Rev. Lett.* **2009**, *102*, 116101.
(54) Kuzmin, M.; Laukkanen, P.; Punkkinen, M. P. J.; Yasir, M.; Tuominen, M.; Dahl, J.; Lång, J. J. K.; Mäkelä, J.; Kokko, K. Atomic Structure and Thermally Induced Transformation of the Crystalline BaO/Si(100) Junction. *Phys. Rev. B* **2014**, *90*, 235405.

DOI: 10.1021/am5089007
ACS Appl. Mater. Interfaces 2015, 7, 6146−6152